Population of Bright Plume Threads in Solar Polar Coronal Holes

Zhenghua Huang[1] · Quanhao Zhang[2] · Lidong Xia[1] · Li Feng[3] · Hui Fu[1] ·
Weixin Liu[1] · Mingzhe Sun[1] · Youqian Qi[1] · Dayang Liu[1] · Qingmin Zhang[3] ·
Bo Li[1]

Abstract Coronal holes are well accepted to be source regions of the fast solar wind. As one
of the common structures in coronal holes, coronal plumes might contribute to the origin of
the nascent solar wind. To estimate the contribution of coronal plumes to the nascent solar
wind, we make the first attempt to estimate their populations in the solar polar coronal holes.
By comparing the observations viewed from two different angles taken by the twin satellites
of STEREO and the results of Monte Carlo simulations, we estimate about $16-27$ plumes
rooted in an area of 4×10^4 arcsec^2 of the polar coronal holes near the solar minimum,
which occupy about $2-3.4\%$ of the area. Based on these values, the contribution of coronal
plumes to the nascent solar wind has also been discussed. A further investigation indicates
that a more precise number of coronal plumes can be worked out with observations from
three or more viewing angles.

1. Introduction

Coronal holes (CHs) are dark areas in the solar corona as viewed in EUV and soft X-ray
passband. They are (almost) permanent structure in the polar region, but can also be seen
in any other location on the Sun (Cranmer, 2009). It is believed that CHs are sources of
fast solar wind, the high speed (> 500 km s^{-1}) component of the stream of plasma in the
interplanetary space flowing outward from the Sun (Krieger, Timothy, and Roelof, 1973).

✉ Z. Huang
z.huang@sdu.edu.cn

1 Shandong Key Laboratory of Optical Astronomy and Solar-Terrestrial Environment, Institute
of Space Sciences, Shandong University, Weihai 264209, Shandong, China

2 CAS Key Laboratory of Geospace Environment, School of Earth and Space Sciences, University
of Science and Technology of China, Hefei 230026, Anhui, China

3 Key Laboratory for Dark Matter and Space Astronomy, Purple Mountain Observatory, CAS,
Nanjing 210034, China
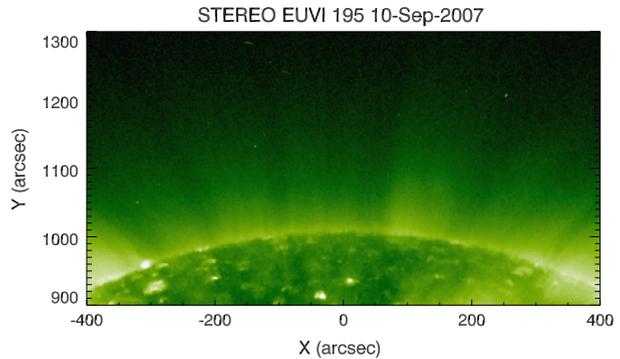
While slow solar wind might come from active regions (see e.g. Brooks et al., 2020), brightenings occurring at the boundaries of CHs also play an important role (Madjarska and Wiegelmann, 2009; Subramanian, Madjarska, and Doyle, 2010; Neugebauer, 2012; Madjarska et al., 2012). Thus, CHs have been intensively studied in order to understand the formation of the nascent solar wind (e.g. Hassler et al., 1999; Xia, Marsch, and Curdt, 2003; Popescu, Doyle, and Xia, 2004; Xia, Marsch, and Wilhelm, 2004; Tu et al., 2005; He et al., 2010).

Although CHs are relatively "quiet" compared to the other places of the solar corona, they are structured with bright points (e.g. Huang et al., 2012; Mou et al., 2016), coronal jets (e.g. Shen et al., 2011; Panesar, Sterling, and Moore, 2018; Kumar et al., 2019; McGlasson et al., 2019) and coronal plumes (e.g. Ahmad and Withbroe, 1977; Yang et al., 2011; Raouafi and Stenborg, 2014), etc. Coronal plumes (CPs) are bright ray-like features that are abundant in CHs (Wilhelm et al., 2011; Poletto, 2015). CPs can be easily seen in the polar CHs where they extend off-limb and thus have a great contrast to the background (see Figure 1). Many studies (e.g. Wang, 1998; Wang and Muglach, 2008; Gabriel et al., 2009; Pucci et al., 2014) have found that CPs in CHs are normally rooted in coronal bright points that are small compact brightenings in the corona with a diameter of 20–30 Mm in average (Madjarska, 2019) or network regions that are lane-like structures in the "quiet" solar chromosphere consisting of numerous fine-scaled active bright dots.

Because CPs usually occur in CHs and apparently extend along the open magnetic field lines, their connection with solar wind has been a major interest of the community. By studying spectroscopic data with the Doppler dimming technique, Gabriel, Bely-Dubau, and Lemaire (2003) found that CPs have outward velocities in excess of 60 km s^{-1} at the heights ranging from 1.05 to 1.35 R$_\odot$ (solar radii) and they estimate that CPs contribute about half of the mass of the fast solar wind at 1.1 R$_\odot$. A further study (Gabriel et al., 2005) suggests that the mass in plumes might transfer to inter-plume regions while they are propagating outward exceeding 1.6 R$_\odot$. More recently, analyses of on-disk plumes revealed that their Doppler velocities increase with heights from 10 km s^{-1} at 1.02 R$_\odot$ to 25 km s^{-1} at 1.05 R$_\odot$, suggesting a significant total of mass balancing the loss by the solar wind (Fu et al., 2014). Using spectral data from UVCS/SOHO and imaging data from LASCO/SOHO, Zangrilli and Giordano (2020) conclude that CPs can contribute about 20% of the solar wind originated from the solar poles. Furthermore, propagating quasi-periodic disturbances whose speeds are more than 100 km s^{-1} usually present in CPs, and they might also play an important role in carrying mass and/or energy from lower solar atmosphere to corona and then power the solar wind (DeForest and Gurman, 1998; Ofman, Nakariakov, and Sehgal, 2000; Gupta et al., 2010; Tian et al., 2011a,b; Krishna Prasad, Banerjee, and Gupta, 2011; Tian et al., 2012;

Jiao et al., 2015; Qi et al., 2019; Cho et al., 2020). However, the contributions of CPs to solar wind is still under debate. Some studies found that inter-plume regions contribute the major part of the mass flowing in the fast solar wind from coronal holes (Wilhelm et al., 2000; Patsourakos and Vial, 2000; Giordano et al., 2000; Teriaca et al., 2003; Feng et al., 2009).

In order to assess the contribution of CPs to the solar wind and/or coronal heating, it is crucial to estimate the ratio of the area occupied by CPs to the whole CH (i.e. the population of CPs). This is especially difficult in the polar region because CPs' emission is optically-thin and the line-of-sight effect brings any CPs in the background and foreground to the same imaging plane as illustrated in Figure 1. As concluded by Gabriel, Bely-Dubau, and Lemaire (2003), CPs apparently make a substantial contribution to the line-of-sight intensity. Such estimation to the population of CPs is impossible-to-some-extent using observations from a single viewing angle, but a solution might be given by multi-angle observations, which have been successfully used to determine the 3D geometry of plumes (Feng et al., 2009; de Patoul et al., 2013) and coronal loops (Feng et al., 2007a,b; Aschwanden et al., 2009; Aschwanden, 2011, 2013), 3D locations of comets (Cheng et al., 2020) and 3D structures of solar winds (Li et al., 2018; Lyu, Li, and Wang, 2020; Li et al., 2020) and coronal mass ejections (Feng et al., 2012; Feng, Inhester, and Mierla, 2013), etc. Here, using observations from the twin STEREO (Solar TErrestrial RElations Observatory) satellites (STEREO-A and STEREO-B, Kaiser et al., 2008), we make the first attempt to estimate the population of CPs in the solar polar coronal holes.

In what follows, we describe observations in Section 2 and methodology and results in Section 3, give prospects in Section 4 and conclusion in Section 5.

2. Observations

The observations analyzed here were achieved by the Extreme Ultraviolet Imager (EUVI, Wuelser et al., 2004) that is part of the Sun Earth Connection Coronal and Heliospheric Investigation (SECCHI, Howard et al., 2008) on-board STEREO. They are subregions of the images with a circular field-of-view up to ±1.7 solar radii taken at the 195 Å passband (representative of temperatures peak at 1.6 MK, Howard et al., 2008). The angular sampling of the images is 1.6″ per pixel. The data include those taken from both the twin satellites of STEREO-A and STEREO-B, on which the EUVI telescopes are designed to be identical. We used the data when the twin satellites are separated for roughly 30°, 60°, 90°, 120° and 150° in the Heliocentric Earth EQuatorial coordinate system (HEEQ, Thompson, 2006). The details of the analyzed data are given in Table 1.

The data are calibrated with the standard procedure of *secchi_prep.pro* provided in the *solar software* by the instrument team. We then use the procedure of *scc_roll_image.pro* to roll and align the images to the Radial-Tangential-Normal (RTN) coordinate system that put the solar north up (Thompson, 2006; Thompson and Wei, 2010). In order to directly compare the two images observed by the two satellites at a given time, the ratio of the distances between the Sun and the satellite for STEREO-A and STEREO-B (see Table 1) are used to reconstruct the images for a pixel of the two images having the same spatial scale on the Sun.

3. Methodology and Results

As mentioned earlier, the line-of-sight effect is the key problem that brings difficulty in determining the population of CPs in the polar CH. More than one distributions of CPs can

Table 1   Details of the data analyzed in the present study and the estimated plume populations based on these observations.

Date YYYYMMDD	Time (UT)	Separation[a] (°)	D_A/D_B[b]	Number of CP threads[c]	Occupancy of CPs[d]
20070910	00:05	30.1	0.888	22	2.8%
20080710	00:05	60.2	0.891	27	3.4%
20090201	00:05	90.4	0.957	$20 \sim 30$	$2.5\% \sim 3.8\%$
20091012	00:05	120.2	0.890	16	2.0%
20100805	00:05	150.2	0.905	20	2.5%

[a]Separation angle between STEREO-A and STEREO-B in HEEQ coordinates.

[b]$D_{A(B)}$ is the distance between STEREO-A(B) and the Sun.

[c]Number of CP threads estimated in an area of $200'' \times 200''$ above polar coronal holes.

[d]Occupancy in area based on the number of CP threads. See the main text for detail.

Figure 2   The north polar cap of the Sun in EUV 195 Å passband observed by SECCHI/EUVI on-board the STEREO-A (left) and STEREO-B (right) while the two satellites are separated by about 30°. A radial filter has been applied on the regions above the limb and the images are shown in logarithm scale. This is an example of the polar region of the Sun studied in the present study. The region enclosed by the dotted lines is used to determine the fine structures of the polar plumes.
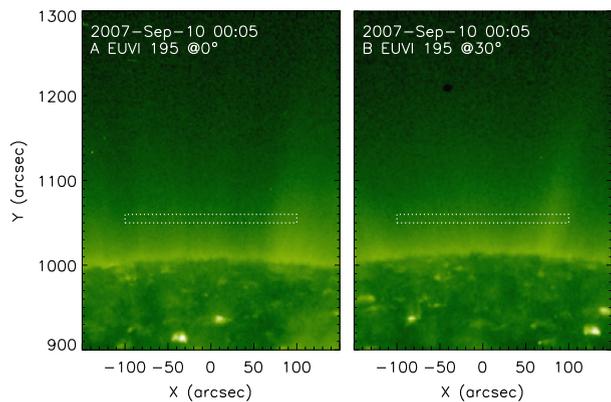
lead to the same observables at a single viewing angle. Thus simultaneous observations from an additional viewing angle can provide extra constraints and potentially give a solution. To find such a solution for achieving the population of CPs, we develop a method based on Monte Carlo simulations. The simulations randomly provide distributions of CPs in a selected region of the solar polar CH, and compute the observables at the corresponding viewing angles. The randomness of the distribution includes the number of CPs and the locations where the CPs rooted in a CH. The correlation coefficients between the simulated observables and those observed by the two satellites are then calculated. The distributions of CPs having correlation coefficients better than 2σ (hereafter, correlation coefficient threshold) above the average of all cases for both viewing angles are then selected as potential solutions.

As the first step, we produce the intensity variation curve (IVC) along solar_X from $-100''$ to $+100''$ (the unit of arcsec is based on STEREO-A) averaging in the solar_Y range of $50 - 60''$ above the north solar limb (see the dotted lines in Figure 2). Such IVCs are obtained from observations taken from both A and B satellites. Because the studied region is off-limb and centering at solar_X=0, the IVCs from both satellites are supposed being from the field-of-views having the same central point. The IVCs are then smoothed with a window of 3 to increase signal-to-noise ratio (see black curves as example in Figure 3). Next,

Figure 3 Examples of intensity variation curves (IVCs) obtained from the STEREO-A (top panel) and STEREO-B (bottom panel) on 2007 September 10 while the two satellites are separated by about 30°. The arcsec units of the X-axis are both scaled to that of STEREO-A. The black lines are the normalized original IVCs and the orange lines are the normalized clean curves generated from the identified local peaks (see the main text for details). The dotted lines in the top panel denote the range of X-axis where four plume threads locate next to each other apparently. Both the original and the clean curves have been normalized to 1 in order to compare them.
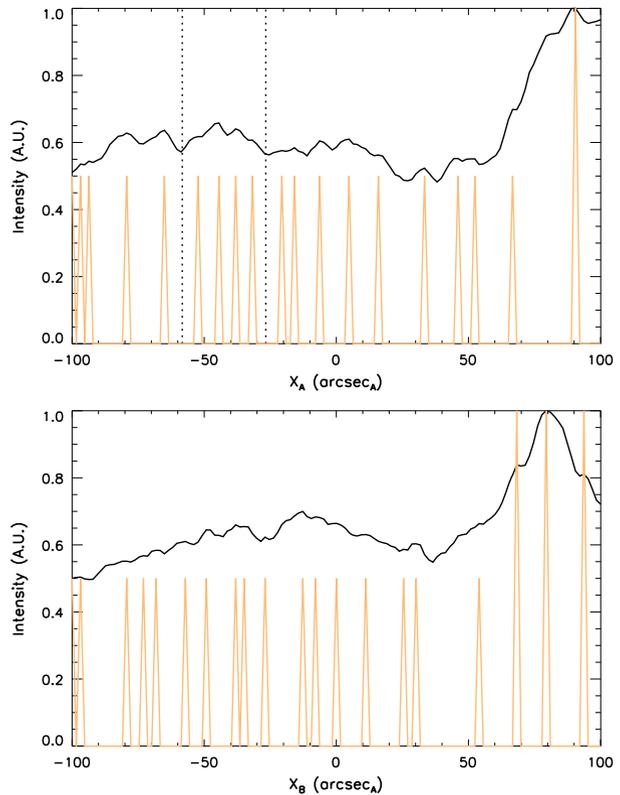
we identify the local peaks (humps) in the IVC using the method on the basis of derivative of the curves as described in previous studies (Huang et al., 2017). The selected solar_Y locations for obtaining the IVC is far from the limb where the intensity of EUVI 195 Å drops to about $1/e$ of the maximum of that at the limb. We have also applied the same procedures on the location range of $90 - 100''$ above the limb, and we obtain similar values (results not shown). We believe that the identified local peaks are corresponding to bright plume threads since most of the omnipresent spicules can only reach a height of about $20''$ (see Sterling, 2000, and the references therein). An array of factors is then determined as the round values of the intensities of the local peaks divided by the minimum of all. For each IVC, we generate a clean curve having the same elements as the original one, in which the locations of local peaks are given the obtained factors and the rest are given as zero (see the orange lines in Figure 3, where 19 peaks are identified in the STEREO-A curve and 20 in the STEREO-B curve). Here we denote the numbers of local peaks identified from the STEREO-A and STEREO-B observations as N_A and N_B, respectively. We then run Monte Carlo simulations by letting the number of plume threads vary from the maximum of $[N_A, N_B]$ to $N_A \times N_B$ and letting the corresponding plumes randomly locate in an area of solar_X $= [-100, 100]$ and solar_Z $= [-100, 100]$ (solar_Z is along line-of-sight at STEREO-A viewing angle). For each selected number of plumes, the simulations consider 10,000 random combinations of their locations. In total, a Monte Carlo simulation for a specific separation of STEREO-A and STEREO-B includes $10^4 \times (N_A \times N_B - \max([N_A, N_B]) + 1)$ random cases, which is 3.61×10^6 for the example shown in Figure 3. In the simulations, each plume is assumed to have intensity of 1. If there are more than one plumes in the same line-of-sight, the

Figure 4   Histograms of number of hits at various guessed number of plumes given in the Monte Carlo simulation based on the observations shown in Figure 3, i.e. the two satellites are separated by 30°. The histogram peaks at the point that the number of plumes is 22. The black curves are the histogram based on each guessed plume number being given 10^4 random combinations of locations, while the orange curves are based on 10^5 random combinations and the number of hits are divided by 10.
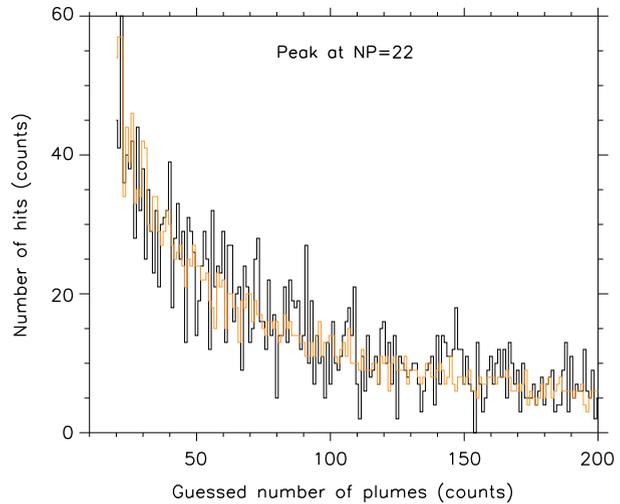
observables sum all of them based on the optically-thin assumption. We can then obtain the simulated IVCs based on a specific viewing angle as determined by the separation of STEREO-A and STEREO-B. The correlation coefficients of the simulated IVCs and the corresponding clean curves based on observations are calculated to determine which plume population(s) can best reproduce the observations. If correlation coefficients based on both STEREO-A and STEREO-B observations meet the criterion mentioned earlier, we denote the corresponding guess as a hit.

In Figure 4, we give histograms of the number of hits varying with the guessed number of plumes. We also show in this case the results while consider 100,000 random distributions of locations of plumes for the simulation (see the orange curves in Figure 4). We can see that the histograms from 10,000 and 100,000 random distributions of locations are giving almost identical results in relative. Therefore, here we simulate only 10,000 cases in order to reduce the consumption of the computing resources. From Figure 4, we can see that a large range of numbers of plumes can reproduce the observations, which is consistent with one's common sense. It is also shown in the histogram that the distribution peaks at a certain guessed number of plumes. We take this guess of number of plumes as the most possible number of plumes in the reality. For the example shown in Figure 4, that is 22. As one can see that this number is close to the number of humps identified in the IVCs, it indicates that CPs are sparse in the polar CH. We would like to note that the correlation coefficient computed here is linear Pearson correlation. Because the curves used for calculations are "clean" with only spikes, such correlation is very sensitive if there is any shift in those spikes, and thus most of the results obtained here are less than 0.5. Even though such correlation coefficients are small, the data numbers are large (125 points in these cases) and thus it is still significant that the two data series are correlated (also see an example in Figure 5). Actually, we have tested the method on artificial data before applied on the observations (see an example shown in the appendix). We found that it is acceptable based on two viewing angles in cases where plumes are not too dense.

In Figure 6, we show the histograms of the number of hits based on the observations while the two satellites are separated by 60°, 90°, 120° and 150°. The best estimated numbers of plumes for the observations at separations of 60°, 120° and 150° are 27, 16 and 20, respectively. Although the simulations based on the observations taken at 90° give the best

Figure 5 A comparison to a simulated curve (blue line) and the observed curve (orange line). The correlation coefficient between the two curves is 0.42.
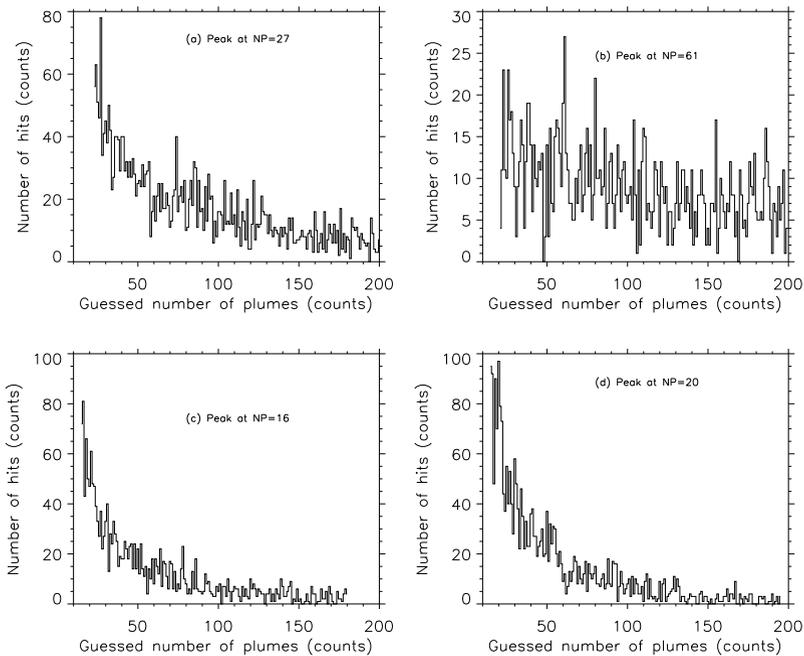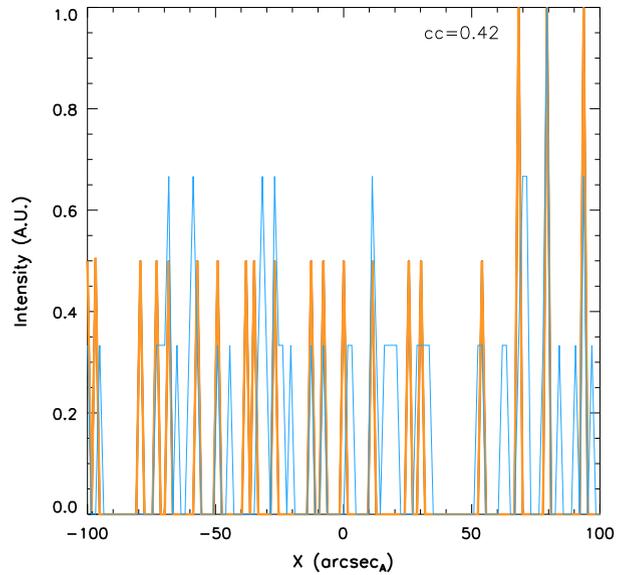
Figure 6 The same as Figure 4, but for the observations while the two satellites are separated by 60° (**a**), 90° (**b**), 120° (**c**) and 150° (**d**).

estimation at the plume number of 61, we see that the numbers of hits are generally higher in the range between 20 and 30, and thus it is reasonable to assume the correct number falling in this range too. These values indicate that plume populations based on these five datasets

are quite close, and this is reasonable as all the observations were taken at the time near the solar minimum.

In Figure 3, we found that some plume threads seemingly locate next to each other on the plane of sky, so that their corresponding peaks in the lightcurves are very close to each other (see the region denoted by the dotted line in Figure 3). It is reasonable to assume that the total of the cross-sections of these plume threads is equivalent to the spatial range in X between the two dips at both sides (see the dotted lines in Figure 3). Based on this assumption, we obtain a good estimation of about 8″ for the cross-sections of the plume threads, which is consistent with that reported in the previous study (Deforest et al., 1997). On the assumption that these plume threads have a cylinder geometry, we can obtain the total area of the solar surface that all the plume threads occupy. Given 20 plume threads, the area is estimated to be about 1,000 arcsec^2. Compared to the total area of CH of the observation and simulations, which is 40,000 arcsec^2, plumes appear to occupy only a small fraction ($\sim$ 2.5%) of the area in the CH. The occupancies of CP threads based on the four datasets range from 2% to 3.4% (see Table 1). Please note that these results can be affected by a few factors, including the resolution and sensitivity of the instruments and the relevant assumptions in our method. For example, the method does not take into account the variety of the width and emission of the plume threads. Therefore, these numbers can be treated as the lower limits of the estimations. Since CPs are rooted in the network lanes, this proportion is half of that of the size of network magnetic elements (representative of the network lane) to a supergranulation (representative of the full network cell), in which the network magnetic elements have a size in the order of 1″ (DeForest et al., 2007; Lamb et al., 2008; Xie et al., 2009; Lamb et al., 2010; Jiang et al., 2020) and the supergranulations have a size of about 30 – 40″ (Rieutord and Rincon, 2010) and both can be assumed to be circular geometries. This suggests that not all network lanes produce CPs, which is consistent with observations (Qi et al., 2019). By taking into account the density of CPs is typically about five times of that of the inter-plume regions (Wilhelm et al., 2011), CPs can contribute about 9 – 15% of the solar winds from the solar poles, which is less than the recent result reported by Zangrilli and Giordano (2020). The obtained values were not taken into account the uncertainty brought in by the method and the difference between the speeds of plasma flows in CPs and that in the inter-plume regions. In the near future, spectroscopic observations of polar CHs from out of the ecliptic plane by Solar Orbiter (Müller et al., 2020; Spice Consortium et al., 2020) shall provide direct measurement of the outflow structures in the polar CHs and thus will give a more precise estimation to the contribution from CPs to the nascent solar wind.

Moreover, plumes are also abundant in on-disk coronal holes (e.g. Wang, Warren, and Muglach, 2016; Avallone et al., 2018). The estimation of area of plumes in coronal holes can be improved by using observations of on-disk coronal holes. This will be considered in a future study by taking into account additional treatments such as background subtraction and projection effect.

4. Prospects

In the present work, we make the first attempt to estimate the population of coronal plume threads in the polar coronal hole based on Monte Carlo simulations and observations taken by the twin STEREO satellites at two different viewing angles. As we can see from the results, the solutions given by the simulation have to be determined from the peaks of the histograms of hits. A question is whether an extra constraint (i.e. observations from the third viewing angle) can help giving a better solution. All these constraints should be taken
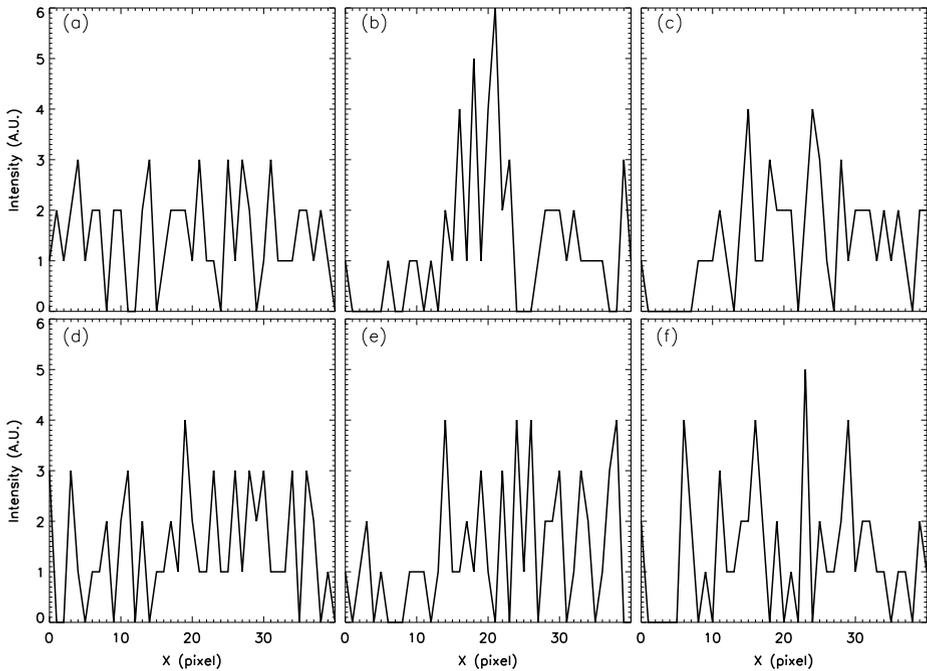
Figure 7 The intensity variation curves of the artificial data with 60 plumes in a region of 40 pixels × 40 pixels viewed at 0° (**a**), 30° (**b**), 60° (**c**), 90° (**d**), 120° (**e**) and 150° (**f**).

with identical instruments like STEREO-A&B, otherwise more free variables should be taken into account. In the Appendix, we have tested a case with sparse plumes and found that observations from three viewing angles give much more promising results. Recently, Wang et al. (2020a,b) propose a concept mission, namely "Solar Ring", for observing the Sun simultaneously from six different viewing angles with duplicated instruments, and we believe such observations shall be powerful in solving the issue here.

Furthermore, here we test another case with much denser plumes, which is based on 60 CPs, each having one pixel width and locating in a region of 40 pixels × 40 pixels (40 pixels perpendicular to line-of-sight and 40 pixels along line-of-sight). In Figure 7, we show the IVCs of the artificial data at a few viewing angles. One can see that the peaks of the IVCs of this case are much denser than those shown in Figure 3. We run similar Monte Carlo simulations based on these intensity variation curves and the histograms of number of hits versus guessed number of plumes are given in Figure 8. The solutions given from two viewing angles (the black curves in Figure 8) show tendency in a few ranges of numbers (see the humps of the red curves in Figure 8), some of which are very close to the correct number. However, the distributions are broad without dominant peaks, and thus they give little confidence for solving the correct number. This is significantly different from the results given in the analyses of the case shown in the appendix and the real observations. The main reason is that the plumes as shown in the IVCs of this case are much denser than those shown in the appendix and the real observations. This indicates that high resolution and high sensitivity data will also help.

While including observations from an additional viewing angle (the orange curves in Figure 8), the distributions of hits are sparse, and thus allow a much better chance for getting the
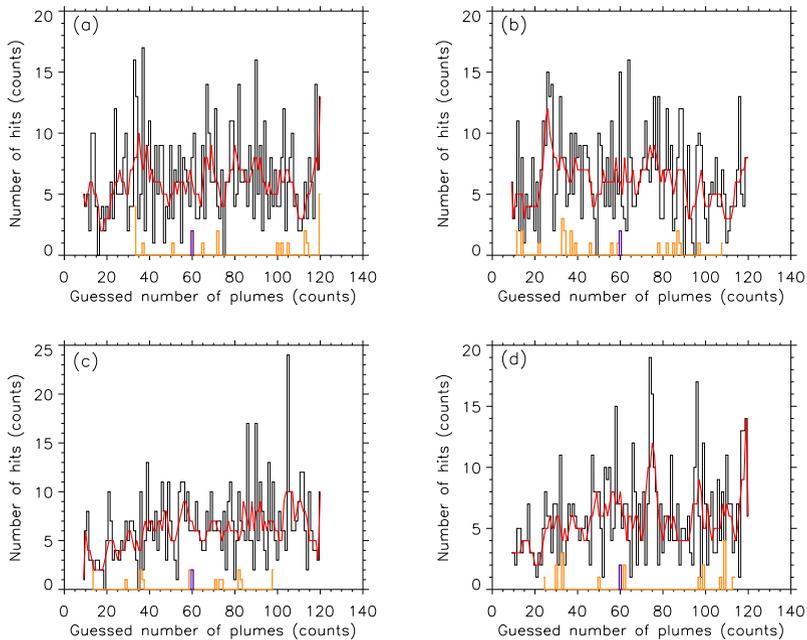
Figure 8 Histograms of number of hits at various guessed number of plumes given in the Monte Carlo simulation based on the artificial data (see Figure 7). Black curves are obtained from two viewing angles and a correlation coefficient threshold of 2σ (**a**: $0°$ & $30°$; **b**: $0°$ & $90°$; **c**: $0°$ & $120°$; **d**: $0°$ & $150°$). Red curves are the black curves smoothed by a window of 5. Orange curves are obtained from three viewing angles and a correlation coefficient threshold of 2σ (**a**: $0°$, $30°$ & $60°$; **b**: $0°$, $30°$ & $90°$; **c**: $0°$, $30°$ & $120°$; **d**: $0°$, $30°$ & $150°$). Blue curves are obtained from three viewing angles as same as the orange curve shown in the same panel but with a correlation coefficient threshold of 3σ.

correct answer. Furthermore, while the correlation coefficient threshold is 3σ, we found the Monte Carlo simulations return exactly the right number (see the blue curves in Figure 8) even though the plumes are relatively dense in the region. This indicates that observations from three different viewing angles can actually solve the problem, but the correlation coefficient threshold has to be carefully selected. Especially in analyses of real observations, it is even more tricky for selection of the threshold. (For example, if a threshold of 3σ is used, no hit will be found in the cases shown in Section 2.) Therefore, to observe the Sun simultaneously from more than two viewing angles like that proposed in the concept of the Solar Ring mission will help distinguish the plasma structures in the corona and the solar wind, even though the structures are quite dense.

5. Conclusion

Coronal plumes (CPs) are one of the common structures rooting in the solar coronal holes where the solar winds are originated. CPs have been thought to contribute significantly to the origin of the solar wind, but that remains under debate. The population of CPs in coronal holes is crucial in understanding their significance. Using the observations from the twin satellites of STEREO and Monte Carlo simulations, here we make the first attempt to estimate the population of CPs above the solar polar coronal holes. We found that CPs occupy
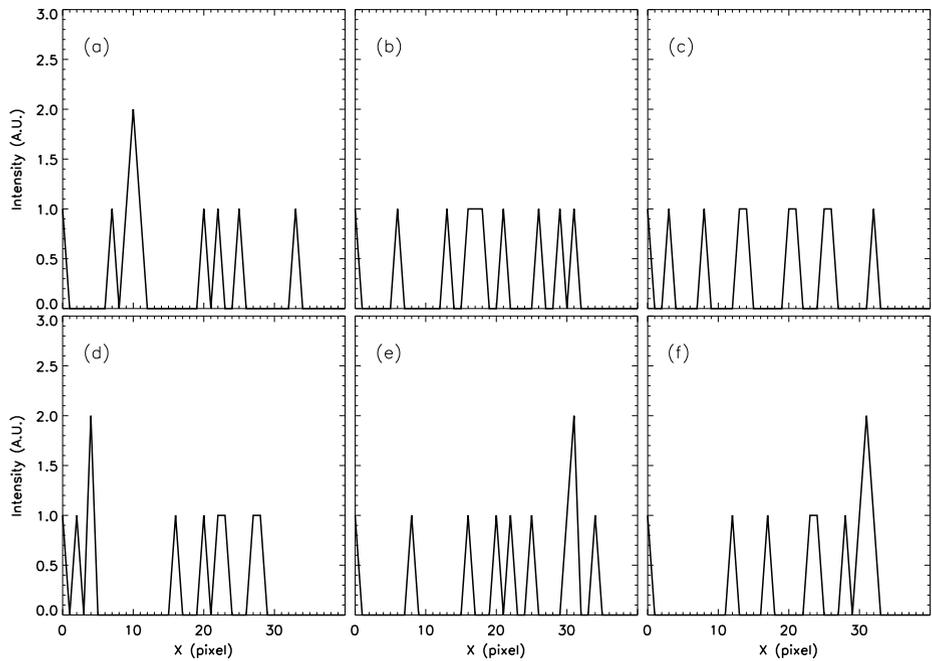
Figure 9 The intensity variation curves of the artificial data with 10 plumes in a region of 40 pixels × 40 pixels viewed at 0° (**a**), 30° (**b**), 60° (**c**), 90° (**d**), 120° (**e**) and 150° (**f**).

about 2 – 3.4% of the area of the polar coronal holes near the solar minimum. We estimate that CPs contribute about 9 – 15% of the solar wind originating in the polar coronal hole. These results could be affected by a few factors, including the resolution and sensitivity of the instruments and relevant assumptions used in the method (e.g. the identification of peaks, the assumption of the identical emission and size of each plume thread and the depth along line-of-sight). Nevertheless, our results indicate that bright plume threads are not the major (in volume) structures of the polar coronal holes and our attempts show that stereoscopic observations could be powerful in resolving structures in the corona.

Our tests using artificial data found that the method can well work out the number of CPs with observations from more than two viewing angles even in the cases that CPs are relatively dense. This demands simultaneous observations of the Sun from identical instruments at various viewing angles as described in the recently proposed Solar Ring mission (Wang et al., 2020a).

Disclosure of Potential Conflicts of Interest   The authors declare that they have no conflicts of interest.

Publisher's Note   Springer Nature remains neutral with regard to jurisdictional claims in published maps and institutional affiliations.
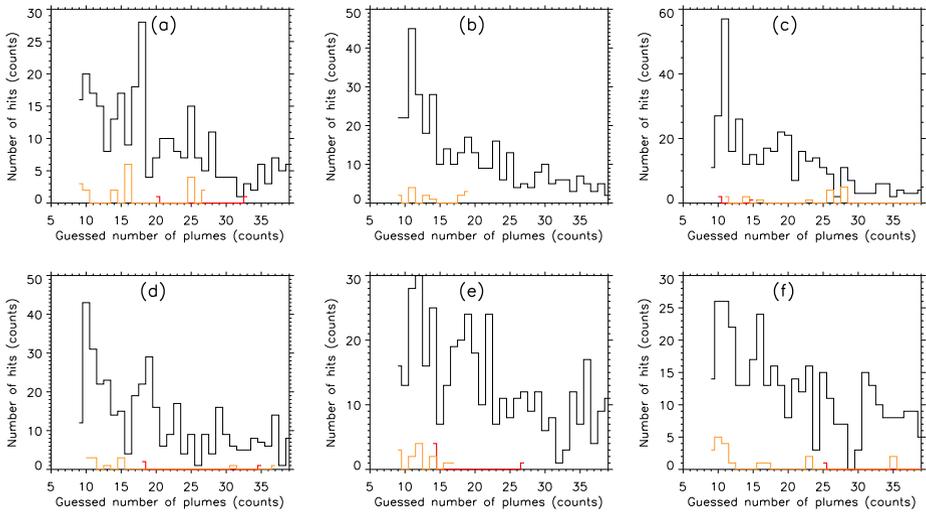
Figure 10 Histograms of number of hits at various guessed number of plumes given in the Monte Carlo simulation based on the artificial data with 10 plumes (see Figure 9). Black curves are obtained from two viewing angles and a correlation coefficient threshold of 2σ (**a**: 0° & 30°; **b**: 0° & 60°; **c**: 0° & 90°; **d**: 0° & 120°; **e**: 0° & 150°; **f**: 60° & 120°). Red curves are based on two viewing angles as same as those used in the black curves but with a correlation coefficient threshold of 3σ. (Red curves are not shown in panel b because none has satisfied the threshold.) Orange curves are obtained from three viewing angles and a correlation coefficient threshold of 2σ (**a**: 0°, 30° & 60°; **b**: 0°, 60° & 90°; **c**: 0°, 30° & 90°; **d**: 0°, 30° & 120°; **e**: 0°, 30° & 150°; **f**: 0°, 60° & 120°).

Appendix: A Test to The Method

In order to test the method as described in Section 2, we apply it on a set of artificial data based on that 10 plumes (each has a size of a pixel) root in an area of 40 pixels × 40 pixels. In Figure 9, we show the IVCs at a set of viewing angles. We can see that in this case the local peaks in the IVCs are sparse, and this is similar to those determined from observations (as shown in Figure 3). In Figure 10, we show the histograms of the distributions of the correlation coefficients derived from the Monte Carlo simulations of these artificial data. We can see that the distributions based on two viewing angles (black curves in Figure 10) show clear dominant peaks near the right number. The numbers of plumes indicated by these dominant peaks are from 10 to 12, except the case based on 0° and 30°. Although the histogram of the case of 0° and 30° has dominant peak at the guessed plume number of 18, the distribution around the plume number of 10 still appears to be larger than the rest in general. Therefore, one can have a good estimation of the number of plumes based on the histograms of the number of hits based on two viewing angles within an error of about 20%. If we increase the correlation coefficient threshold to 3σ, we can see that very few (even none) hits can be obtained (see the red curves in Figure 10). It appears that one cannot get a better estimation of the plume number based on this threshold than that from 2σ.

While we include additional data from a third viewing angle, we found that the histograms of the number of hits using a threshold of 2σ distribute at a few isolated numbers including one really close to the correct one (see the orange curves in Figure 10). Although this does not work out the exact answer, it gives a much better chance if one has to give a guess. If we are increasing the threshold further, the data from three viewing angles can derive a unique number that is very close to the answer at some point. However, we fail to find a universal threshold for all, and that seems to be different from case to case.

References

Ahmad, I.A., Withbroe, G.L.: 1977, EUV analysis of polar plumes. *Solar Phys.* **53**, 397. DOI. ADS.

Spice Consortium, Anderson, M., Appourchaux, T., Auchère, F., Aznar Cuadrado, R., Barbay, J., Baudin, F., Beardsley, S., Bocchialini, K., Borgo, B., Bruzzi, D., Buchlin, E., Burton, G., Büchel, V., Caldwell, M., Caminade, S., Carlsson, M., Curdt, W., Davenne, J., Davila, J., Deforest, C.E., Del Zanna, G., Drummond, D., Dubau, J., Dumesnil, C., Dunn, G., Eccleston, P., Fludra, A., Fredvik, T., Gabriel, A., Giunta, A., Gottwald, A., Griffin, D., Grundy, T., Guest, S., Gyo, M., Haberreiter, M., Hansteen, V., Harrison, R., Hassler, D.M., Haugan, S.V.H., Howe, C., Janvier, M., Klein, R., Koller, S., Kucera, T.A., Kouliche, D., Marsch, E., Marshall, A., Marshall, G., Matthews, S.A., McQuirk, C., Meining, S., Mercier, C., Morris, N., Morse, T., Munro, G., Parenti, S., Pastor-Santos, C., Peter, H., Pfiffner, D., Phelan, P., Philippon, A., Richards, A., Rogers, K., Sawyer, C., Schlatter, P., Schmutz, W., Schühle, U., Shaughnessy, B., Sidher, S., Solanki, S.K., Speight, R., Spescha, M., Szwec, N., Tamiatto, C., Teriaca, L., Thompson, W., Tosh, I., Tustain, S., Vial, J.-C., Walls, B., Waltham, N., Wimmer-Schweingruber, R., Woodward, S., Young, P., de Groof, A., Pacros, A., Williams, D., Müller, D.: 2020, The Solar Orbiter SPICE instrument. An extreme UV imaging spectrometer. *Astron. Astrophys.* **642**, A14. DOI. ADS.

Aschwanden, M.J.: 2011, Solar stereoscopy and tomography. *Living Rev. Solar Phys.* **8**, 5. DOI. ADS.

Aschwanden, M.J.: 2013, Nonlinear force-free magnetic field fitting to coronal loops with and without stereoscopy. *Astrophys. J.* **763**, 115. DOI. ADS.

Aschwanden, M.J., Wuelser, J.-P., Nitta, N.V., Lemen, J.R., Sandman, A.: 2009, First three-dimensional reconstructions of coronal loops with the STEREO A+B spacecraft. III. Instant stereoscopic tomography of active regions. *Astrophys. J.* **695**, 12. DOI. ADS.

Avallone, E.A., Tiwari, S.K., Panesar, N.K., Moore, R.L., Winebarger, A.: 2018, Critical magnetic field strengths for solar coronal plumes in quiet regions and coronal holes? *Astrophys. J.* **861**, 111. DOI. ADS.

Brooks, D.H., Winebarger, A.R., Savage, S., Warren, H.P., De Pontieu, B., Peter, H., Cirtain, J.W., Golub, L., Kobayashi, K., McIntosh, S.W., McKenzie, D., Morton, R., Rachmeler, L., Testa, P., Tiwari, S., Walsh, R.: 2020, The drivers of active region outflows into the slow solar wind. *Astrophys. J.* **894**, 144. DOI. ADS.

Cheng, L., Zhang, Q., Wang, Y., Li, X., Liu, R.: 2020, Using stereoscopic observations of cometary plasma tails to infer solar wind speed. *Astrophys. J.* **897**, 87. DOI. ADS.

Cho, I.-H., Nakariakov, V.M., Moon, Y.-J., Lee, J.-Y., Yu, D.J., Cho, K.-S., Yurchyshyn, V., Lee, H.: 2020, Accelerating and supersonic density fluctuations in coronal hole plumes: signature of nascent solar winds. *Astrophys. J. Lett.* **900**, L19. DOI. ADS.

Cranmer, S.R.: 2009, Coronal holes. *Living Rev. Solar Phys.* **6**, 3. DOI. ADS.

de Patoul, J., Inhester, B., Feng, L., Wiegelmann, T.: 2013, 2D and 3D polar plume analysis from the three vantage positions of STEREO/EUVI A, B, and SOHO/EIT. *Solar Phys.* **283**, 207. DOI. ADS.

DeForest, C.E., Gurman, J.B.: 1998, Observation of quasi-periodic compressive waves in solar polar plumes. *Astrophys. J. Lett.* **501**, L217. DOI. ADS.

Deforest, C.E., Hoeksema, J.T., Gurman, J.B., Thompson, B.J., Plunkett, S.P., Howard, R., Harrison, R.C., Hassler, D.M.: 1997, Polar plume anatomy: results of a coordinated observation. *Solar Phys.* **175**, 393. DOI. ADS.

DeForest, C.E., Hagenaar, H.J., Lamb, D.A., Parnell, C.E., Welsch, B.T.: 2007, Solar magnetic tracking. I. Software comparison and recommended practices. *Astrophys. J.* **666**, 576. DOI. ADS.

Feng, L., Inhester, B., Mierla, M.: 2013, Comparisons of CME morphological characteristics derived from five 3D reconstruction methods. *Solar Phys.* **282**, 221. DOI. ADS.

Feng, L., Inhester, B., Solanki, S.K., Wiegelmann, T., Podlipnik, B., Howard, R.A., Wuelser, J.-P.: 2007a, First stereoscopic coronal loop reconstructions from STEREO SECCHI images. *Astrophys. J. Lett.* **671**, L205. DOI. ADS.

Feng, L., Wiegelmann, T., Inhester, B., Solanki, S., Gan, W.Q., Ruan, P.: 2007b, Magnetic stereoscopy of coronal loops in NOAA 8891. *Solar Phys.* **241**, 235. DOI. ADS.

Feng, L., Inhester, B., Solanki, S.K., Wilhelm, K., Wiegelmann, T., Podlipnik, B., Howard, R.A., Plunkett, S.P., Wuelser, J.P., Gan, W.Q.: 2009, Stereoscopic polar plume reconstructions from STEREO/SECCHI images. *Astrophys. J.* **700**, 292. DOI. ADS.

Feng, L., Inhester, B., Wei, Y., Gan, W.Q., Zhang, T.L., Wang, M.Y.: 2012, Morphological evolution of a three-dimensional coronal mass ejection cloud reconstructed from three viewpoints. *Astrophys. J.* **751**, 18. DOI. ADS.

Fu, H., Xia, L., Li, B., Huang, Z., Jiao, F., Mou, C.: 2014, Measurements of outflow velocities in on-disk plumes from EIS/Hinode observations. *Astrophys. J.* **794**, 109. DOI. ADS.

Gabriel, A.H., Bely-Dubau, F., Lemaire, P.: 2003, The contribution of polar plumes to the fast solar wind. *Astrophys. J.* **589**, 623. DOI. ADS.

Gabriel, A.H., Abbo, L., Bely-Dubau, F., Llebaria, A., Antonucci, E.: 2005, Solar wind outflow in polar plumes from 1.05 to 2.4 R$_{solar}$. *Astrophys. J. Lett.* **635**, L185. DOI. ADS.

Gabriel, A., Bely-Dubau, F., Tison, E., Wilhelm, K.: 2009, The structure and origin of solar plumes: network plumes. *Astrophys. J.* **700**, 551. DOI. ADS.

Giordano, S., Antonucci, E., Noci, G., Romoli, M., Kohl, J.L.: 2000, Identification of the coronal sources of the fast solar wind. *Astrophys. J. Lett.* **531**, L79. DOI. ADS.

Gupta, G.R., Banerjee, D., Teriaca, L., Imada, S., Solanki, S.: 2010, Accelerating waves in polar coronal holes as seen by EIS and SUMER. *Astrophys. J.* **718**, 11. DOI. ADS.

Hassler, D.M., Dammasch, I.E., Lemaire, P., Brekke, P., Curdt, W., Mason, H.E., Vial, J.-C., Wilhelm, K.: 1999, Solar wind outflow and the chromospheric magnetic network. *Science* **283**, 810. DOI. ADS.

He, J.-S., Tu, C.-Y., Tian, H., Marsch, E.: 2010, Solar wind origins in coronal holes and in the quiet Sun. *Adv. Space Res.* **45**, 303. DOI. ADS.

Howard, R.A., Moses, J.D., Vourlidas, A., Newmark, J.S., Socker, D.G., Plunkett, S.P., Korendyke, C.M., Cook, J.W., Hurley, A., Davila, J.M., Thompson, W.T., St. Cyr, O.C., Mentzell, E., Mehalick, K., Lemen, J.R., Wuelser, J.P., Duncan, D.W., Tarbell, T.D., Wolfson, C.J., Moore, A., Harrison, R.A., Waltham, N.R., Lang, J., Davis, C.J., Eyles, C.J., Mapson-Menard, H., Simnett, G.M., Halain, J.P., Defise, J.M., Mazy, E., Rochus, P., Mercier, R., Ravet, M.F., Delmotte, F., Auchere, F., Delaboudiniere, J.P., Bothmer, V., Deutsch, W., Wang, D., Rich, N., Cooper, S., Stephens, V., Maahs, G., Baugh, R., McMullin, D., Carter, T.: 2008, Sun Earth Connection Coronal and Heliospheric Investigation (SECCHI). *Space Sci. Rev.* **136**, 67. DOI. ADS.

Huang, Z., Madjarska, M.S., Doyle, J.G., Lamb, D.A.: 2012, Coronal hole boundaries at small scales. IV. SOT view. Magnetic field properties of small-scale transient brightenings in coronal holes. *Astron. Astrophys.* **548**, A62. DOI. ADS.

Huang, Z., Madjarska, M.S., Scullion, E.M., Xia, L.-D., Doyle, J.G., Ray, T.: 2017, Explosive events in active region observed by IRIS and SST/CRISP. *Mon. Not. Roy. Astron. Soc.* **464**, 1753. DOI. ADS.

Jiang, H., Wang, J., Liu, C., Jing, J., Liu, H., Wang, J.T.L., Wang, H.: 2020, Identifying and tracking solar magnetic flux elements with deep learning. *Astrophys. J. Suppl.* **250**, 5. DOI. ADS.

Jiao, F., Xia, L., Li, B., Huang, Z., Li, X., Chandrashekhar, K., Mou, C., Fu, H.: 2015, Sources of quasi-periodic propagating disturbances above a solar polar coronal hole. *Astrophys. J. Lett.* **809**, L17. DOI. ADS.

Kaiser, M.L., Kucera, T.A., Davila, J.M., St. Cyr, O.C., Guhathakurta, M., Christian, E.: 2008, The STEREO mission: an introduction. *Space Sci. Rev.* **136**, 5. DOI. ADS.

Krieger, A.S., Timothy, A.F., Roelof, E.C.: 1973, A coronal hole and its identification as the source of a high velocity solar wind stream. *Solar Phys.* **29**, 505. DOI. ADS.

Krishna Prasad, S., Banerjee, D., Gupta, G.R.: 2011, Propagating intensity disturbances in polar corona as seen from AIA/SDO. *Astron. Astrophys.* **528**, L4. DOI. ADS.

Kumar, P., Karpen, J.T., Antiochos, S.K., Wyper, P.F., DeVore, C.R., DeForest, C.E.: 2019, Multiwavelength study of equatorial coronal-hole jets. *Astrophys. J.* **873**, 93. DOI. ADS.

Lamb, D.A., DeForest, C.E., Hagenaar, H.J., Parnell, C.E., Welsch, B.T.: 2008, Solar magnetic tracking. II. The apparent unipolar origin of quiet-Sun flux. *Astrophys. J.* **674**, 520. DOI. ADS.

Lamb, D.A., DeForest, C.E., Hagenaar, H.J., Parnell, C.E., Welsch, B.T.: 2010, Solar magnetic tracking. III. Apparent unipolar flux emergence in high-resolution observations. *Astrophys. J.* **720**, 1405. DOI. ADS.

Li, X., Wang, Y., Liu, R., Shen, C., Zhang, Q., Zhuang, B., Liu, J., Chi, Y.: 2018, Reconstructing solar wind inhomogeneous structures from stereoscopic observations in white light: small transients along the Sun-Earth line. *J. Geophys. Res.* **123**, 7257. DOI. ADS.

Li, X., Wang, Y., Liu, R., Shen, C., Zhang, Q., Lyu, S., Zhuang, B., Shen, F., Liu, J., Chi, Y.: 2020, Reconstructing solar wind inhomogeneous structures from stereoscopic observations in white light: solar wind transients in 3-D. *J. Geophys. Res.* **125**, e27513. DOI. ADS.

Lyu, S., Li, X., Wang, Y.: 2020, Optimal stereoscopic angle for reconstructing solar wind inhomogeneous structures. *Adv. Space Res.* **66**, 2251. DOI. ADS.

Madjarska, M.S.: 2019, Coronal bright points. *Living Rev. Solar Phys.* **16**, 2. DOI. ADS.

Madjarska, M.S., Wiegelmann, T.: 2009, Coronal hole boundaries evolution at small scales. I. EIT 195 Å and TRACE 171 Å view. *Astron. Astrophys.* **503**, 991. DOI. ADS.

Madjarska, M.S., Huang, Z., Doyle, J.G., Subramanian, S.: 2012, Coronal hole boundaries evolution at small scales. III. EIS and SUMER views. *Astron. Astrophys.* **545**, A67. DOI. ADS.

McGlasson, R.A., Panesar, N.K., Sterling, A.C., Moore, R.L.: 2019, Magnetic flux cancellation as the trigger mechanism of solar coronal jets. *Astrophys. J.* **882**, 16. DOI. ADS.

Mou, C., Huang, Z., Xia, L., Madjarska, M.S., Li, B., Fu, H., Jiao, F., Hou, Z.: 2016, Magnetic flux supplement to coronal bright points. *Astrophys. J.* **818**, 9. DOI. ADS.

Müller, D., St. Cyr, O.C., Zouganelis, I., Gilbert, H.R., Marsden, R., Nieves-Chinchilla, T., Antonucci, E., Auchère, F., Berghmans, D., Horbury, T.S., Howard, R.A., Krucker, S., Maksimovic, M., Owen, C.J.,

Rochus, P., Rodriguez-Pacheco, J., Romoli, M., Solanki, S.K., Bruno, R., Carlsson, M., Fludra, A., Harra, L., Hassler, D.M., Livi, S., Louarn, P., Peter, H., Schühle, U., Teriaca, L., del Toro Iniesta, J.C., Wimmer-Schweingruber, R.F., Marsch, E., Velli, M., De Groof, A., Walsh, A., Williams, D.: 2020, The Solar Orbiter mission. Science overview. *Astron. Astrophys.* **642**, A1. DOI. ADS.

Neugebauer, M.: 2012, Evidence for polar X-ray jets as sources of microstream peaks in the solar wind. *Astrophys. J.* **750**, 50. DOI. ADS.

Ofman, L., Nakariakov, V.M., Sehgal, N.: 2000, Dissipation of slow magnetosonic waves in coronal plumes. *Astrophys. J.* **533**, 1071. DOI. ADS.

Panesar, N.K., Sterling, A.C., Moore, R.L.: 2018, Magnetic flux cancelation as the trigger of solar coronal jets in coronal holes. *Astrophys. J.* **853**, 189. DOI. ADS.

Patsourakos, S., Vial, J.-C.: 2000, Outflow velocity of interplume regions at the base of Polar Coronal Holes. *Astron. Astrophys.* **359**, L1. ADS.

Poletto, G.: 2015, Solar coronal plumes. *Living Rev. Solar Phys.* **12**, 7. DOI. ADS.

Popescu, M.D., Doyle, J.G., Xia, L.D.: 2004, Network boundary origins of fast solar wind seen in the low transition region? *Astron. Astrophys.* **421**, 339. DOI. ADS.

Pucci, S., Poletto, G., Sterling, A.C., Romoli, M.: 2014, Birth, life, and death of a solar coronal plume. *Astrophys. J.* **793**, 86. DOI. ADS.

Qi, Y., Huang, Z., Xia, L., Li, B., Fu, H., Liu, W., Sun, M., Hou, Z.: 2019, On the relation between transition region network jets and coronal plumes. *Solar Phys.* **294**, 92. DOI. ADS.

Raouafi, N.-E., Stenborg, G.: 2014, Role of transients in the sustainability of solar coronal plumes. *Astrophys. J.* **787**, 118. DOI. ADS.

Rieutord, M., Rincon, F.: 2010, The Sun's supergranulation. *Living Rev. Solar Phys.* **7**, 2. DOI. ADS.

Shen, Y., Liu, Y., Su, J., Ibrahim, A.: 2011, Kinematics and fine structure of an unwinding polar jet observed by the Solar Dynamic Observatory/Atmospheric Imaging Assembly. *Astrophys. J. Lett.* **735**, L43. DOI. ADS.

Sterling, A.C.: 2000, Solar spicules: a review of recent models and targets for future observations – (invited review). *Solar Phys.* **196**, 79. DOI. ADS.

Subramanian, S., Madjarska, M.S., Doyle, J.G.: 2010, Coronal hole boundaries evolution at small scales. II. XRT view. Can small-scale outflows at CHBs be a source of the slow solar wind. *Astron. Astrophys.* **516**, A50. DOI. ADS.

Teriaca, L., Poletto, G., Romoli, M., Biesecker, D.A.: 2003, The nascent solar wind: origin and acceleration. *Astrophys. J.* **588**, 566. DOI. ADS.

Thompson, W.T.: 2006, Coordinate systems for solar image data. *Astron. Astrophys.* **449**, 791. DOI. ADS.

Thompson, W.T., Wei, K.: 2010, Use of the FITS world coordinate system by STEREO/SECCHI. *Solar Phys.* **261**, 215. DOI. ADS.

Tian, H., McIntosh, S.W., Habbal, S.R., He, J.: 2011a, Observation of high-speed outflow on plume-like structures of the quiet Sun and coronal holes with Solar Dynamics Observatory/Atmospheric Imaging Assembly. *Astrophys. J.* **736**, 130. DOI. ADS.

Tian, H., McIntosh, S.W., De Pontieu, B., Martínez-Sykora, J., Sechler, M., Wang, X.: 2011b, Two components of the solar coronal emission revealed by extreme-ultraviolet spectroscopic observations. *Astrophys. J.* **738**, 18. DOI. ADS.

Tian, H., McIntosh, S.W., Wang, T., Ofman, L., De Pontieu, B., Innes, D.E., Peter, H.: 2012, Persistent Doppler shift oscillations observed with Hinode/EIS in the solar corona: spectroscopic signatures of Alfvénic waves and recurring upflows. *Astrophys. J.* **759**, 144. DOI. ADS.

Tu, C.-Y., Zhou, C., Marsch, E., Xia, L.-D., Zhao, L., Wang, J.-X., Wilhelm, K.: 2005, Solar wind origin in coronal funnels. *Science* **308**, 519. DOI. ADS.

Wang, Y.-M.: 1998, Network activity and the evaporative formation of polar plumes. *Astrophys. J. Lett.* **501**, L145. DOI. ADS.

Wang, Y.-M., Muglach, K.: 2008, Observations of low-latitude coronal plumes. *Solar Phys.* **249**, 17. DOI. ADS.

Wang, Y.-M., Warren, H.P., Muglach, K.: 2016, Converging supergranular flows and the formation of coronal plumes. *Astrophys. J.* **818**, 203. DOI. ADS.

Wang, Y., Ji, H., Wang, Y., Xia, L., Shen, C., Guo, J., Zhang, Q., Huang, Z., Liu, K., Li, X., Liu, R., Wang, J., Wang, S.: 2020a, Concept of the Solar Ring mission: an overview. *Sci. China, Technol. Sci.* **63**, 1699. DOI. ADS.

Wang, Y., Chen, X., Wang, P., Qiu, C., Wang, Y., Zhang, Y.: 2020b, Concept of the Solar Ring mission: preliminary design and mission profile. *Sci. China, Technol. Sci.* DOI.

Wilhelm, K., Dammasch, I.E., Marsch, E., Hassler, D.M.: 2000, On the source regions of the fast solar wind in polar coronal holes. *Astron. Astrophys.* **353**, 749. ADS.

Wilhelm, K., Abbo, L., Auchère, F., Barbey, N., Feng, L., Gabriel, A.H., Giordano, S., Imada, S., Llebaria, A., Matthaeus, W.H., Poletto, G., Raouafi, N.-E., Suess, S.T., Teriaca, L., Wang, Y.-M.: 2011, Morphology,

dynamics and plasma parameters of plumes and inter-plume regions in solar coronal holes. *Astron. Astrophys. Rev.* **19**, 35. DOI. ADS.

Wuelser, J.-P., Lemen, J.R., Tarbell, T.D., Wolfson, C.J., Cannon, J.C., Carpenter, B.A., Duncan, D.W., Gradwohl, G.S., Meyer, S.B., Moore, A.S., Navarro, R.L., Pearson, J.D., Rossi, G.R., Springer, L.A., Howard, R.A., Moses, J.D., Newmark, J.S., Delaboudiniere, J.-P., Artzner, G.E., Auchere, F., Bougnet, M., Bouyries, P., Bridou, F., Clotaire, J.-Y., Colas, G., Delmotte, F., Jerome, A., Lamare, M., Mercier, R., Mullot, M., Ravet, M.-F., Song, X., Bothmer, V., Deutsch, W.: 2004, EUVI: the STEREO-SECCHI extreme ultraviolet imager. In: Fineschi, S., Gummin, M.A. (eds.) *Telescopes and Instrumentation for Solar Astrophysics*, *Society of Photo-Optical Instrumentation Engineers (SPIE) Conference Series* **5171**, 111. DOI. ADS.

Xia, L.D., Marsch, E., Curdt, W.: 2003, On the outflow in an equatorial coronal hole. *Astron. Astrophys.* **399**, L5. DOI. ADS.

Xia, L.D., Marsch, E., Wilhelm, K.: 2004, On the network structures in solar equatorial coronal holes. Observations of SUMER and MDI on SOHO. *Astron. Astrophys.* **424**, 1025. DOI. ADS.

Xie, Z.X., Yu, D.R., Zhang, J., Yang, S.H., Hu, Q.H.: 2009, Properties of magnetic elements in the quiet Sun using the marker-controlled watershed method. *Astron. Astrophys.* **505**, 801. DOI. ADS.

Yang, S., Zhang, J., Zhang, Z., Zhao, Z., Liu, Y., Song, Q., Yang, S., Bao, X., Li, L., Chu, Z., Li, T.: 2011, Polar plumes observed at the total solar eclipse in 2009. *Sci. China Ser. G, Phys. Mech. Astron.* **54**, 1906. DOI. ADS.

Zangrilli, L., Giordano, S.M.: 2020, Contribution of polar plumes to fast solar wind. *Astron. Astrophys.* **643**, A104. DOI. ADS.